

BSEC method for unveiling open clusters and its application to Gaia

DR3: 83 new clusters

Zhong-Mu Li¹ and Cai-Yan Mao¹

Institute of Astronomy and Information, Dali University, Dali 671003, PR China; *zhongmuli@126.com*

Received 20xx month day; accepted 20xx month day

Abstract Open clusters (OCs) are common in the Milky Way, but most of them remain undiscovered. There are numerous techniques, including some machine-learning algorithms, available for the exploration of OCs. However, each method has its limitations and therefore, different approaches to discovering OCs hold significant value. We develop a comprehensive approach method to automatically explore the data space and identify potential OC candidates with relatively reliable membership determination. This approach combines the techniques of HDBSCAN, GMM, and a novel cluster member identification technique, color excess constraint. The new method exhibits efficiency in detecting OCs while ensuring precise determination of cluster memberships. Because the main feature of this technique is to add an extra constraint for the members of cluster candidates using the homogeneity of color excess, comparing to typical blind search codes, it is called Blind Search-Extra Constraint (BSEC) method. It is successfully applied to the Gaia Data Release 3, and 83 new OCs are found, whose CMDs are fitted well. In addition, this study reports 621 new OC candidates with discernible main sequence or red giant branch. It is shown that BSEC technique can discard some false negatives of previous works, which takes about 3 percentage of known clusters. It shows that as an extra constraint, color excess (or 2-color) constraint is useful for removing fake cluster member stars from the clusters that are identified from the positions and proper motions of stars, and getting more precise CMDs, when differential reddening of member stars of a cluster is not large (e.g., $\Delta E(G_{BP}-G_{RP}) < 0.5$ mag). It makes the CMDs of 15 percent clusters clearer (in particular for the region near turnoff) and therefore is helpful for CMD and stellar population studies. Our result suggests that color excess constraint is more appropriate for clusters with small differential reddening, such as globular clusters or older OCs, and clusters that the distances of member stars can not be determined accurately.

Key words: Galaxy: stellar content – (Galaxy:) open clusters and associations: general –

1 INTRODUCTION

Open clusters (OCs) are widely recognized as valuable laboratories for studying stellar evolution and as tracers of the structure of the Milky Way galaxy. They serve as excellent subjects for investigating stellar evolution because stars with the same metallicity and age locate on an isochrone including different stellar evolutionary stages. In addition, they provide valuable insights into Galactic structure through the observation and measurement of numerous distant OCs and their respective stellar properties. Consequently, extensive efforts have been dedicated to searching for OCs using diverse datasets, resulting in a significant increase in the number of identified OCs (Hunt & Reffert 2023) following the release of Gaia data (Gaia Collaboration et al. 2016, 2018, 2021, 2023) in recent years. The number of well-known OCs are now more than 3000 (see, e.g., Castro-Ginard et al. 2022 and Hunt & Reffert 2023). However, the number of known OCs is still significantly lower than the predicted value (> 10000 , Minniti 2023). Besides the limitation of observational data, the technique for searching for OCs plays an important role. Notably, following the substantial increase in the size of OC samples, which was achieved by Mermillod (1995) (1200 OCs), the largest increase to the number of Galactic OCs came with the application of new searching methods. For example, the OC number of the catalogue of Kharchenko et al. (2013) (hereafter MWSC) reached 2267. The recent rise in OC numbers can be attributed to both Gaia data releases and advancements in algorithms designed for identifying these clusters. A lot of studies, including Castro-Ginard et al. (2018, 2019, 2020, 2022) (CG sample, including 2838 clusters) Liu & Pang (2019), Sim et al. (2019), and Cantat-Gaudin et al. (2019), Li et al. (2022), Hao et al. (2021), He et al. (2021, 2022b,a); Hunt & Reffert (2023); Qin et al. (2023) have reported the discovery of over a few thousand candidate OCs based on Gaia data. Some famous unsupervised machine learning algorithms, e.g., Density-Based Spatial Clustering of Applications with Noise (DBSCAN) (Ester et al. 1996), (Hierarchical Density-Based Spatial Clustering of Applications with Noise (HDBSCAN) (Campello et al. 2013), Gaussian mixture model (GMM) (Dempster et al. 1977), Unsupervised Photometric Membership Assignment in Stellar Clusters (UPMASK) (Krone-Martins & Moitinho 2014; Pera et al. 2021) and friend-of-friend (FoF) (Yang et al. 2005), were employed for blind searches in the Gaia dataset to effectively identify OCs. However, none of these algorithms is flawless in terms of both efficiency and precision as highlighted by previous studies (see, e.g., Hunt & Reffert 2021). During testing these algorithms, some known clusters were not detected while fake clusters were occasionally reported. Each method has its own advantages and disadvantages. According to some tests, GMM is good for determining the cluster membership in a small region whereas HDBSCAN is more suitable for searching OCs on a large scale (Hunt & Reffert 2021). DBSCAN is also effective for identifying OCs with similar density (Castro-Ginard et al. 2019). FoF seems nice for large-scale blind search, but it often reports false positives like HDBSCAN does. If membership probabilities are required then GMM and UPMASK can be utilized accordingly. In order to develop an efficient and relatively precise method for searching OCs we conducted this study. The work aims to build a new star cluster search method, Blind Search-Extra Constraint (BSEC), which makes use the advantages of two kinds of existing methods and a new cluster member constraint. The structure of this paper is as follows. In section 2 the design of the new method is

2021). Then in section 4 the crossmatch result and CMDs of new OCs are shown. Finally in section 5 we conclude this work.

2 DESIGN OF BSEC METHOD

When design the BSEC method, the advantages of a few different methods are combined. It comes true by the following steps. First, an effective algorithm is taken to find out star cluster candidates as many as possible. HDBSCAN and FoF are ideal such algorithms. Second, a re-identification algorithm is used to re-identify the OC candidates and remove some fake member stars (i.e., field stars). This step makes the cluster catalogue and member stars of a cluster more reliable. This is important for other works. Finally, an Extra Constraint (EC) algorithm is used to constrain the member stars again based on some well-known knowledge of star clusters. In this work, we used the knowledge that all member stars of a cluster have the similar color excess, besides the similar space coordinates and proper motion. When stars have the same color excess and their color is not too red, metallicity and age, they will distribute on a fixed curve in a color-color diagram (CCD) and on a curve in a color-magnitude diagram (CMD). Fig. 1 shows the CCD of all stars in the PARSEC-COLIBRI isochrone database (Marigo et al. 2017). These stars cover large ranges in metallicity ($0.0002 \leq Z \leq 0.05$) and age ($3.98 \text{ Myr} \leq \text{age} \leq 13.2 \text{ Gyr}$). We see clearly that when the colors of stars are not too red, e.g., $G_{BP} - G \leq 3.0$ or $G_{BP} - G_{RP} \leq 2.0$, the color-color relation (CCR) of stars can be described well using a polynomial function, with an uncertainty of about 0.05 mag. For most redder stars, their CCR can also be described via the same fitting function. As we see, the fitting CCR is almost independent on the mass, age, and metallicity of stars. There is a fixed fitting function for a group of stars if they have the same color excess, although the fitting formulae are different for various color excesses. This is very the case of a star cluster, because the member stars have the same color excess for any fixed color. We can therefore apply the CCR to give a new constraint on the member stars of a cluster. Stars that distribute near the CCR of a cluster are possibly the members of the cluster, while those far from the CCR are not. Any two colors can be used for building the CCR of a cluster. In this work, we take $(G_{BP} - G)$ and $(G_{BP} - G_{RP})$ to build the CCRs. For a fixed cluster that is observed by Gaia satellite, the CCR is similar to those shown in Fig. 2. Note that the observed CCR is different from that of PARSEC-COLIBRI stellar isochrones, because of the color excesses in two colors. We can kick out the stars that are obviously distant from the CCR curve, as they are not possible the members of cluster. This technique is called color excess constraint or 2-color constraint. It is thought as the first part of extra constraint (EC) of star clusters. Our experiment shows that 2-color constraint kicks out a lot of fake clusters or stars with large photometric uncertainties.

However, the CCR is affected by differential reddening, which may result in significant error when CCR is used. In order to test how differential reddening affects the CCR, we calculate the CCRs with maximum differential reddening values $\Delta E(G_{BP}-G_{RP})$ from 0.1 to 1.5 mag. Fig. 3 shows two examples that take the maximum differential reddening values of 0.5 and 1.0 mag. In the figure, purple squares are stars with random differential reddening $\Delta E(G_{BP}-G_{RP})$ lower than 0.5 mag. The orange line is the fitting relation of these stars, while the blue dashed lines denote an error of 0.05 mag around the fitting curve. We can see

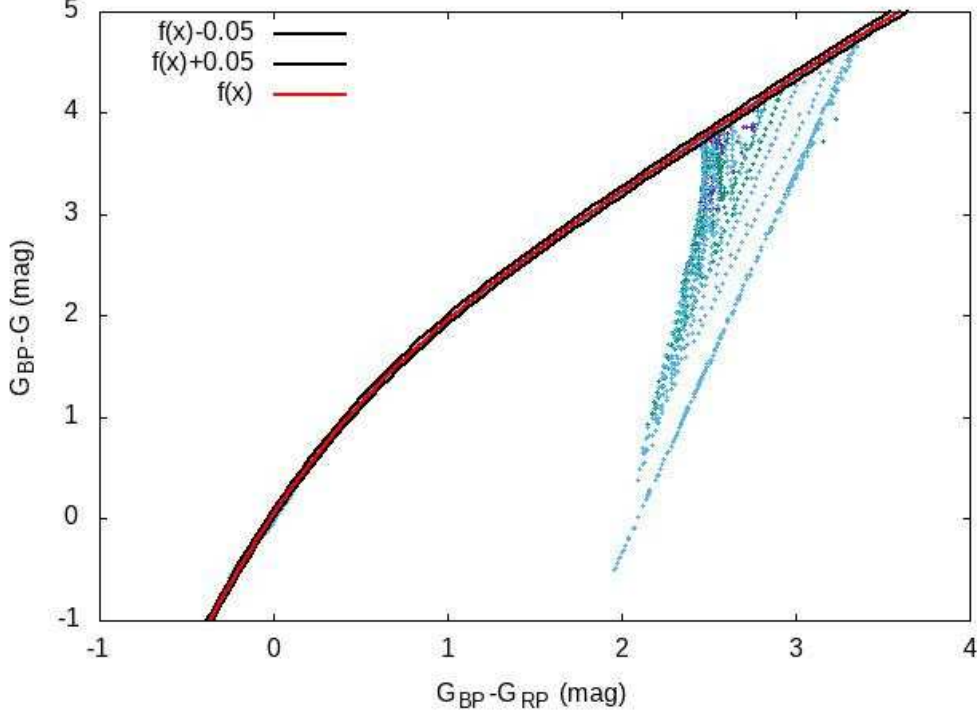


Fig. 1: Color-color diagram of stars in the PARSEC-COLIBRI isochrone database. The metallicity (Z) of stars covers the range of 0.0002 to 0.05, while the age of stars covers the range of 3.98 Myr to 13.2 Gyr. Points denote stars in the isochrone database. Red line shows the fitting function $f(x) = 0.0456 + 2.5451x - 0.8290x^2 + 0.2193x^3 - 0.0220x^4$, while black lines show an uncertainty of 0.05 mag.

by the differential reddening. Gray dots are for stars with differential reddening smaller than 1.0 mag. It shows that the color dispersion is significantly larger than the case of differential reddening of 0.5 mag. Table 1 lists the errors of fitting CCRs when taking different values for maximum differential reddening. We observe that the fitting error of CCR increases with differential reddening. It can be concluded that CCR is an effective method for constraining member stars of star cluster when differential reddening is not large, e.g., $\Delta E(G_{BP}-G_{RP}) < 0.5$ mag. Therefore, it is more suitable for studying globular clusters and OCs older than 0.3 Gyr because of the rare gas and dust. In other words, the color excess constraint may not be appropriate for star clusters with large differential reddening, except there is obvious difference between the reddennings of cluster member stars and the others. According to the CMDs of the 83 newly discovered OCs in this work, the color spread of main sequence stars near the turn-off is not larger than about 0.6 mag (including a spread of 0.1 mag caused by binaries) or that of red giant stars is lower than 0.5 mag. It suggests that the differential reddening of these OCs is likely smaller than 0.5 mag. Thus the CCR can be used for

Table 1: The errors of best fitting CCRs when taking different values of maximum differential reddening of stars. $\Delta E(G_{BP}-G_{RP})_{\max}$ is for the value of maximum differential reddening.

$\Delta E(G_{BP}-G_{RP})_{\max}$ [mag]	error [mag]
0.1	0.01
0.2	0.01
0.3	0.02
0.4	0.03
0.5	0.05
0.6	0.07
0.7	0.10
0.8	0.12
0.9	0.14
1.0	0.17
1.1	0.20
1.2	0.25
1.3	0.30
1.4	0.34
1.5	0.40

3 APPLICATION OF BSEC METHOD TO GAIA DR3

3.1 Blind search of OC candidates

3.1.1 Data

This work uses the data of the latest release of Gaia, i.e., Gaia DR3 (Gaia Collaboration et al. 2023). It contains the astrometry and broad-band photometry already published as part of Gaia EDR3 (Gaia Collaboration et al. 2021). This release supplies more stars and more accurate astrometric and photometric data comparing with the first and second releases (DR1 and DR2) (Gaia Collaboration et al. 2016, 2018). No cuts is applied on the observational data, because we need to find out OC candidates as many as possible. In total, this catalogue contains relatively accurate astrometry and photometry for more than 1.5 billion sources (Forveille & Kotak 2021; Gaia Collaboration et al. 2021; Damjanovic 2021; Gaia Collaboration et al. 2023). As is well-known, Gaia data have been widely used in the studies of star clusters.

3.1.2 Algorithm for blind search

The famous cluster search algorithm, HDBSCAN, is used for blind search of OC candidates. HDBSCAN is a clustering algorithm that can be used to find cluster candidates in various densities. This makes it possible to find some small clusters that contains tens of member stars and suitable for this work. A minimum cluster size mcl_{size} is set to 25, rather than the suggested value 10, because a mcl_{size} of 10 results to too many cluster candidates, which are much more than previous findings. The leaf mode rather than the default mode (Excess of Mass, i.e., EoM) is taken, because this mode is more effective. In addition, two candidates

method may combined two clusters with different distances incorrectly, so we will check the results with parallax distribution later. Because this is a test, we take each original data file of Gaia DR3 as a grid for blind search. Although it is somewhat rough, it will not affect the final result obviously, as each file covers enough large coordinate space.

3.1.3 Result

The blind search of HDBSCAN reports 6908 cluster candidates. The candidate number is similar to a recent work, Hunt & Reffert (2023). However, as pointed by some papers, e.g., Hunt & Reffert (2023), there are possibly many fake positive identifications in the results of HDBSCAN. In addition, the CMDs of some candidates seem strange or contains too many stars (more than 1 million) because no cut is applied on the observational data. This makes the results not enough reliable and it is impossible to use the data for other researches directly. Therefore, a re-identification based on the HDBSCAN results have to be done.

3.2 Re-identification of member stars

3.2.1 GMM re-identification

The GMM algorithm is used to re-identify the cluster candidates, because it is powerful for detecting the cluster members and can supply the possibilities of stars. Here some cuts are applied on the results of HDBSCAN, for each cluster candidate. In detail, stars are constrained to be brighter than 21 mag, with parallax between 0 and 7 mas and proper motions (μ_α^* and μ_δ) between -50 and 50 mas/yr. In order to make the results more reliable, only stars around the mean values of proper motions, parallax and coordinates are selected for GMM re-identification. This kicks out most field stars and make the re-identification much faster and effective. After the re-identification, we can choose member stars of a cluster according to their possibilities. As examples, Figs. 4 and 5 show the distributions of member stars after HDBSCAN and GMM processes, in the coordinate and CMD spaces. We can see that the CMDs become closer to the isochrones of stellar populations if taking larger (e.g, 0.5 and 0.9) possibility cuts (examples 2 and 3 of Fig. 5). In this work, we take a possibility cut of 0.9 to make sure the member stars reliable. Cluster candidates that have preferable CMDs, which include at least main sequence or red giant branch, are studied here, because their CMDs can be compared to stellar isochrones (e.g., Marigo et al. 2017) and therefore the age and (or) metallicity of such candidates can possibly be determined. These candidates are more likely to be star clusters. As a result, 5411 cluster candidates with more than 20 member stars are obtained by the GMM re-identification, within which 1166 ones have preferable CMDs.

3.2.2 Extra constraint

Because the main structure of CMDs (e.g., main sequence branch, turn off and red giant branch) of some cluster candidates remains unclear and the astrometric parameters of member stars of some candidates distribute dispersively, an EC constraint is applied to the results of GMM re-identification results. This process is based on the member stars with GMM possibilities larger than 0.9. As the first part of extra

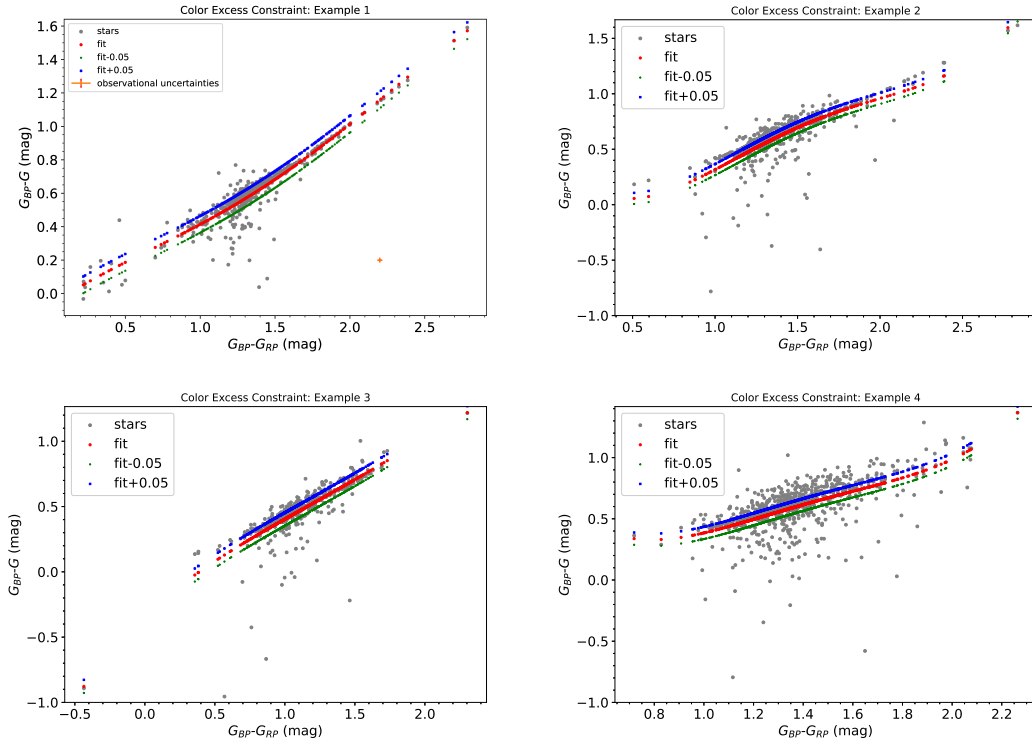


Fig. 2: Color excess constraint (or 2-color constraint) of member stars of clusters, which is based on the color-color relation of stars with the same color excess. If there is no observational error, member stars of a cluster should be on a curve like where the red points locate at. The gray and red points are for the observed and fitted results. The blue and green points indicate the possible range of stars of a cluster if an uncertainty of 0.05 mag is taken for the colors. Only stars distributing between this range are taken as members of a cluster. Error bars denote the color uncertainties at 21 mag.

Colors ($G_{BP} - G_{RP}$) and ($G_{BP} - G$) are used for the work. As shown in Fig. 2, only stars within the possible range are taken as member stars of a cluster. An uncertainty of 0.05 mag is taken for stars, because the fitting of the CCR of stars in the PARSEC-COLIBRI isochrone database shows that almost all stars distribute in this range if stars are not too red ($G_{BP} - G \leq 3.0$, see Fig. 1). Note that the four examples shown in Fig. 2 are chosen randomly and therefore are not named. This constraint eliminates some stars that are possibly not cluster members but it does not change the spatial distribution of stars (Fig. 4). The CMDs become clearer after 2-color constraint, as we see in Fig. 5. This will make the CMD fitting of clusters more reliable. We see that some faint stars are removed from cluster members by the 2-color constraint. This may relate to their relative large photometry uncertainties. In particular, some fake blue stragglers (on the upper left of turnoff) are kicked out by the 2-color constraint (examples 2 and 3). This is helpful for both CMD fitting studies and blue straggler studies of star clusters. Note that there is no clear understanding of how the CCR of blue stragglers differ from normal stars, but according to a test based on the data of Cummings & Kalirai (2018), blue stragglers obey the same fitting CCR ($U - B$ vs $B - V$) of all stars if the photometric uncertainties and differential reddening are taken into account. This constraint is also helpful for getting the real red giant branch (see the upper right of example 2). Because the position of

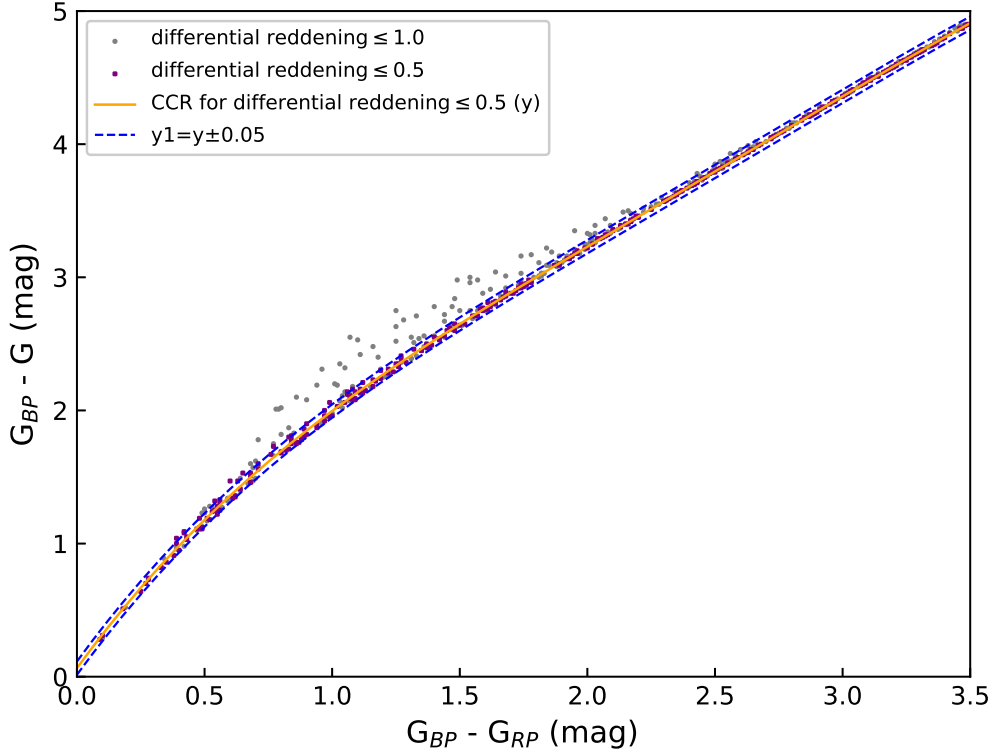


Fig. 3: Example of color dispersions when taking maximum differential reddening $\Delta E(G_{BP}-G_{RP})_{\max}$ of 0.5 and 1.0 mag. Purple squares are stars with random differential reddening lower than 0.5 mag. Orange line is the fitting relation of these stars, while blue dashed lines denote an error of 0.05 mag around the fitting curve. Gray dots are for stars with differential reddening smaller than 1.0 mag.

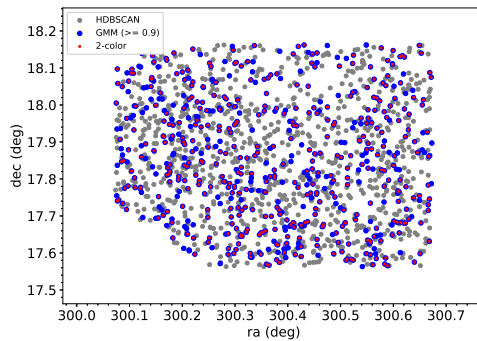


Fig. 4: Distribution of member stars after HDBSCAN, GMM, and 2-color constraint processes.

determining the metallicities of clusters. Thereby, the color excess constraint is useful for getting reliable metallicity, as it helps to obtain more reliable red giant branch. The CMDs of 15% clusters in our work becomes clearer after the 2-color constraint. However, the CMDs of many cluster candidates are not similar to isochrones of stellar populations yet. Such candidates may be not real clusters. We therefore check the CMDs of all candidates, as the second part of extra constraint. The G versus $(G_{BP} - G_{RP})$ CMD is taken

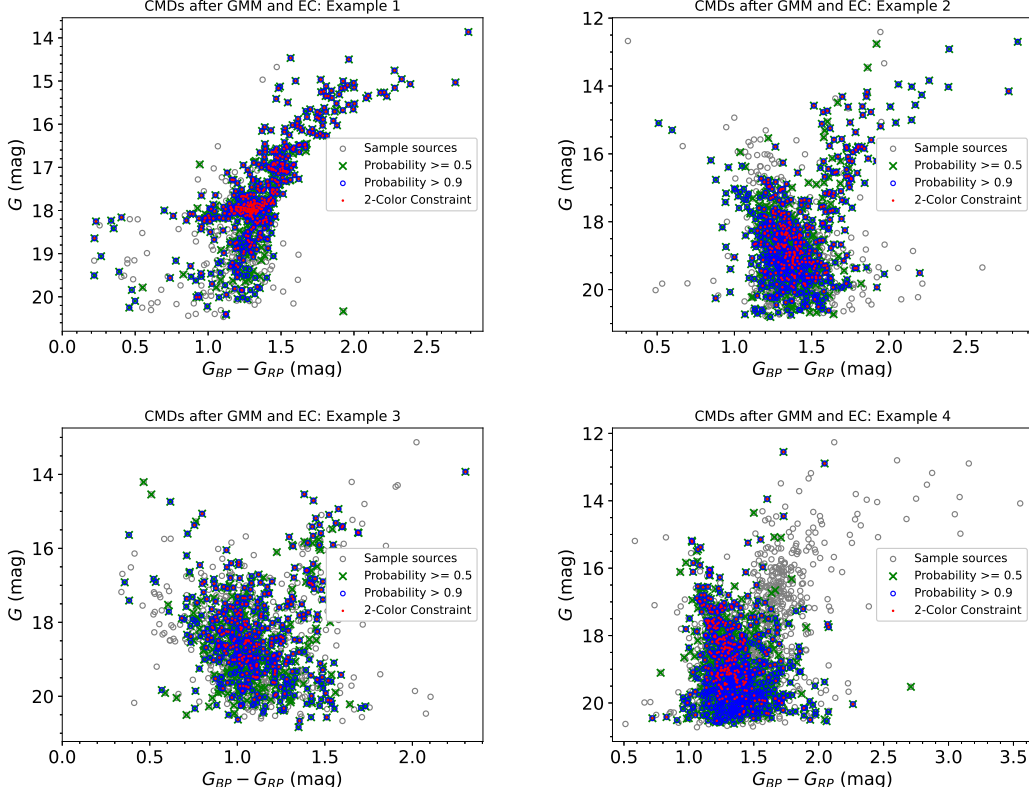


Fig. 5: CMDs of cluster member stars after HDBSCAN (gray open circle), GMM (green cross and blue circle), and 2-color constraint (red point) processes. Stars with two lower limits (0.5 and 0.9) of possibilities are shown for the GMM results.

clear CMDs. Besides these, the final clusters are checked by the proper motion dispersions, via the method of Cantat-Gaudin & Anders (2020) and Hao et al. (2022). Equation 1 is used to judge whether a candidate is real cluster or not. This equation is taken here because newly found clusters have parallax less than about 1 mas.

$$\sqrt{\sigma_{\mu_{\alpha^*}}^2 + \sigma_{\mu_{\delta}}^2} \leq 0.5 \text{ mas.yr}^{-1} \quad (\varpi < 1 \text{ mas}) \quad (1)$$

4 CROSSMATCH TO KNOWN CLUSTERS AND NEWLY FOUND OCS

When we crossmatch the OC candidates to many catalogs of known open clusters or candidates (e.g., Castro-Ginard et al. 2018, 2019, 2020, 2022; Bica et al. 2001; Dias et al. 2002; Reylé & Robin 2002; Bica et al. 2003; Porras et al. 2003; Chen et al. 2003; Frinchaboy et al. 2004; Glushkova et al. 2010; Kharchenko et al. 2013; Schmeja et al. 2014; Camargo et al. 2015; Scholz et al. 2015; Camargo et al. 2016a,b; Kos et al. 2018; Ryu & Lee 2018; Ferreira et al. 2019; Kounkel & Covey 2019; Cantat-Gaudin et al. 2020; Ferreira et al. 2021; Hao et al. 2021; He et al. 2021; Hunt & Reffert 2021; Dias et al. 2021; Hao et al. 2022; Castro-Ginard et al. 2022; Li et al. 2022; He et al. 2022b,a; Chi et al. 2023; Li & Mao 2023; Qin et al. 2023) and globular clusters, 2941 known clusters or candidates (e.g., NGC 5904, NGC 6005, NGC 2420, NGC 6830, NGC 4590, NGC 6584, NGC 6819, NGC 2627, Alessi 6, UBC 285, King 6 and Gulliver 59)

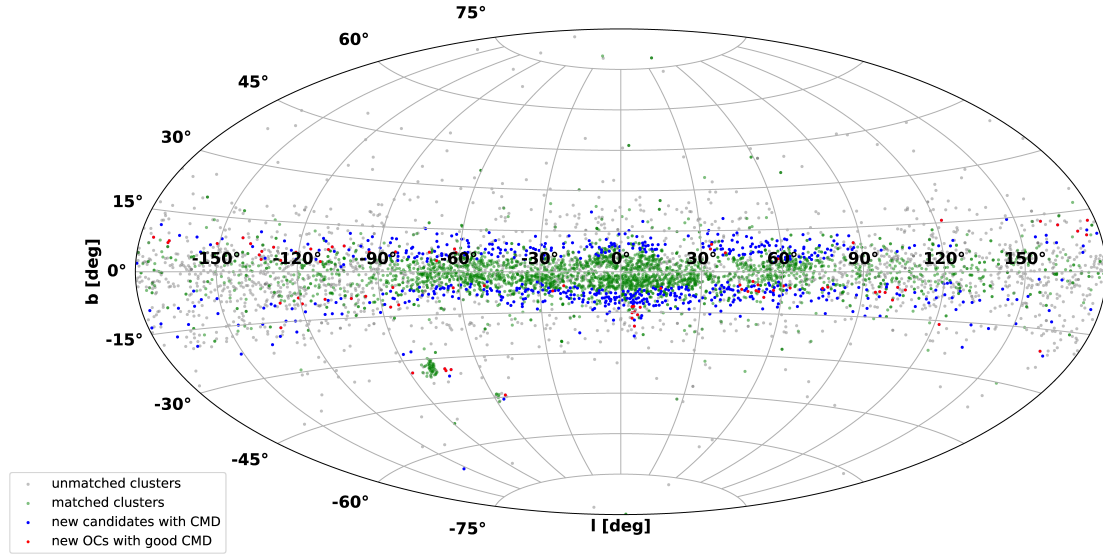


Fig. 6: Distribution of 83 newly found OCs (red) and 621 newly found candidates (blue) in the Galactic coordinate system, together with 2941 matched known clusters and candidates (green) and 2105 unmatched clusters and candidates (grey). The original number of unmatched known clusters is much larger but many clusters are thought as the same one if they are closer than 0.5 deg.

CMDs, 621 ones with rough CMDs, which include at least main sequence or red giant branch and have somewhat large disposition, are found to be new. In particular, 83 ones with good CMDs, which have small disposition and are similar to the isochrones in the PARSEC-COLIBRI database, are found to be new. Because the distributions of the position, proper motion, color excess, and membership possibility of the member stars of each cluster candidate have been constrained in the previous steps, the CMD can be employed to impose an additional constraint on these candidates to identify real clusters. Thus the 83 candidates with good CMDs are more likely to be real clusters. Their stellar populations can be possibly determined from CMDs. We take them as new OCs. The new clusters are judged according to not only their good CMDs, but also the distributions of the position, proper motion, color excess and membership probability. Note that if the distance between the centers of a candidate and a known cluster is less than 0.5 deg, the candidate is thought as a known (or matched) one. Tables 2 and 3 list the numbers of candidates of this work that are matched to known star clusters or candidates in previous catalogs, for all candidates and those with preferable CMDs respectively. Fig. 6 shows the distribution of matched and unmatched known clusters and candidates, together with all newly found candidates with preferable CMDs and clusters with good CMDs in the Galactic coordinate system. We see clearly that the newly found clusters and known clusters are not overlapped. Table 4 shows the known clusters that are not recovered by this work, while Tables 5 and 6 list the astrometric parameters of newly found OCs with good CMDs. Meanwhile, Fig. 7 shows the distributions of galactic longitudes and galactic latitudes of matched and unmatched known clusters. We observe that the most matched clusters distribute around $l = 0 \pm 75$ deg and $b = 0 \pm 10$ deg. It is noted that the number clusters is sensitive to the input parameter of HDBSCAN, `mclSize`. If a smaller value such as 20 or 10 is taken for searching cluster candidates, much more clusters will be reported. In that

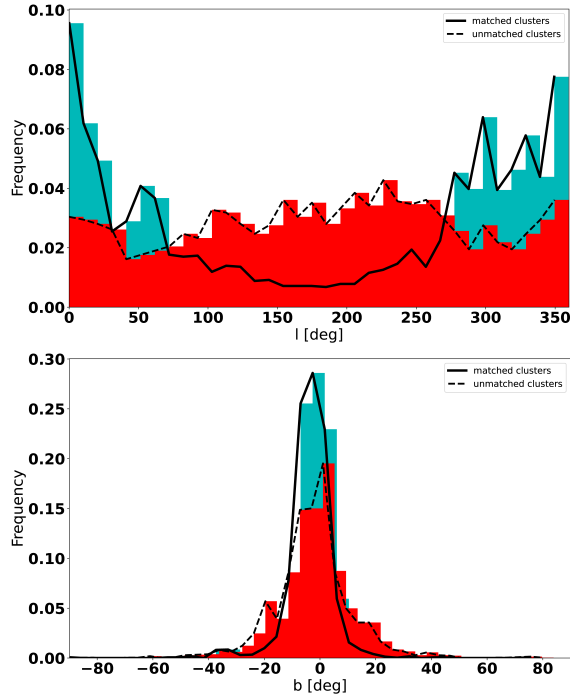


Fig. 7: Distributions of galactic longitudes and galactic latitudes of matched and unmatched known clusters.

As mentioned above, the clusters with similar ra and dec but different ϖ maybe combined into a cluster incorrectly, so we check our results via the parallax of member stars in each cluster. The parallaxes of stars are divided into 5 or 10 bins, according to the star members of clusters, we find that none of the parallax distributions of 83 new clusters exhibits clearly separate bimodal distribution. It can also be checked via the distribution of member stars in the parallax versus proper motion space (Fig. 8). This suggests that the member stars of each cluster distribute in a concentrated area. Therefore, none of the 83 new clusters includes two physically separated clusters.

In order to understand the properties of the newly discovered OCs, we present the distribution of them in different spaces. Fig. 8 shows the distribution of some example newly found OCs in the coordinate, proper motion, proper motion versus parallax, and CMD spaces. Here, we plot stars in the parallax versus proper motion space to check whether the stars can be divided into two groups via parallax, and to check the relation between the two parameters. As we see, most OCs with clear CMDs have clustering features in these spaces. Figs. 9–11 present the proper motion and parallax distributions of newly found OCs (two samples for those with rough CMDs and good CMDs), together with those of the CG sample (Castro-Ginard et al. 2018, 2019, 2020, 2022). We observe that the distributions of proper motion μ_{α^*} and parallax ϖ are different for three samples. It indicates that the fraction of distant OCs is larger in the sample of newly found OCs comparing to the CG sample. Thus BSEC is able to find some distant OCs.

4.1 CMDs of OCs

CMD is an important tool for studying OCs. Many fundamental cluster parameters such as color excess, metallicity, age and binary fraction can be determined from CMDs. Although the CMDs of 83 newly found

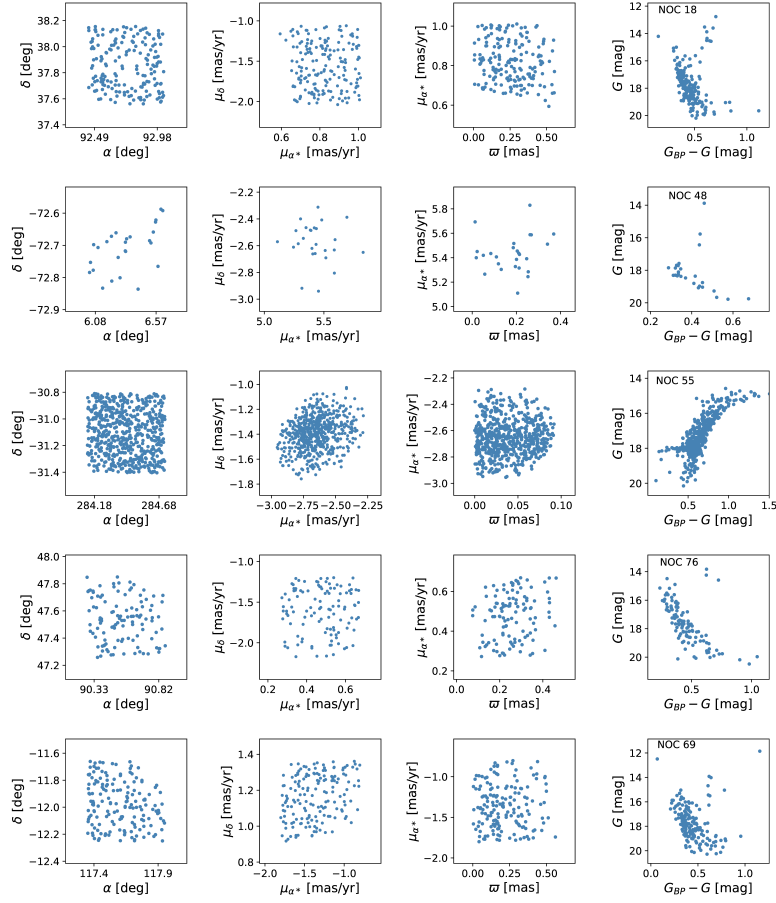


Fig. 8: Distribution of five newly found OCs in the coordinate, proper motion, proper motion versus parallax, and CMD spaces.

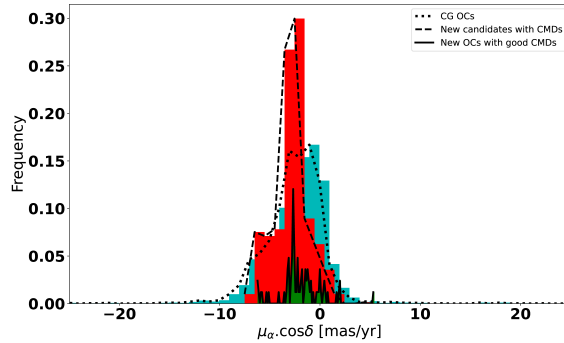


Fig. 9: Comparison of the proper motion distribution ($\mu_\alpha \cos \delta$) of the newly found OC samples with that of CG sample (dotted line). The dashed and solid lines are for OCs with rough CMDs and good CMDs, respectively.

clusters have only main sequence or red giant branch. Although their parallaxes suggest that they should be Milky Way clusters, but there are actually obvious uncertainties in the parallaxes. Figs. 12–14 present the CMDs of the newly found OCs. The fundamental parameters, such as distance modulus, metallicity and age

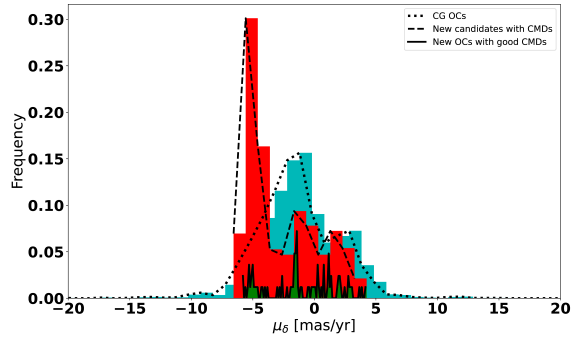


Fig. 10: Similar to Fig. 9, but for another direction (μ_δ).

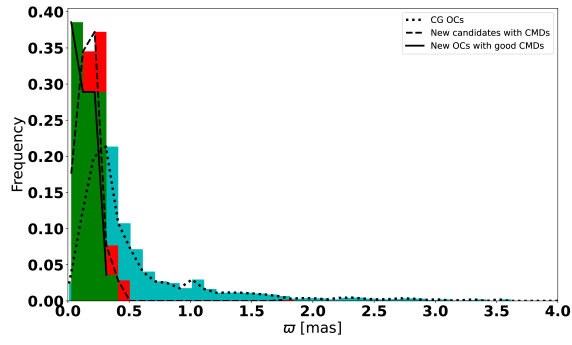


Fig. 11: Comparison of the parallax distributions of the newly found OC sample and that of CG sample.

CMD fitting of these clusters will be done and reported in another paper using the stellar population model and CMD fitting code of Li et al. (2017) and Li et al. (2021).

5 CONCLUSION

This paper brings forward a new composed method, BSEC, for hunting for star clusters. The main feature of BSEC is that cluster members are constrained by not only proper motions, space coordinates, but also the color excess and CMD shape. The fitted curve of color-color relation is used for constraining the member stars of a cluster when the maximum differential reddening of stars in a cluster is not too large. This color excess constraint technique improves obviously the membership of clusters and help to obtain clearer CMDs of about 15% clusters. However, the constraint cannot be independently used for cluster identification. It is better to use it as an extra constraint (EC) of cluster members. Moreover, the EC technique is probably useful for star clusters that the distances of member stars are not determined accurately. It can be used for finding out the background and foreground stars, as their reddening is usually different from cluster members. The BSEC method is then applied to the data of Gaia DR3. It finally found 83 new OCs with CMDs similar to the isochrones of stellar populations and 621 new candidates with rough CMDs. It is worth noting that the space distributions in the *ra* versus *dec* space of a few cluster candidates not similar to circles because of the limitation of the observed files used for the study, but this does not affect the conclusion, because this work aims to introduce new methods, BSEC and color excess constraint. Moreover, we take the number of known real clusters as 3000, BSEC method will discard some false negatives of previous works,

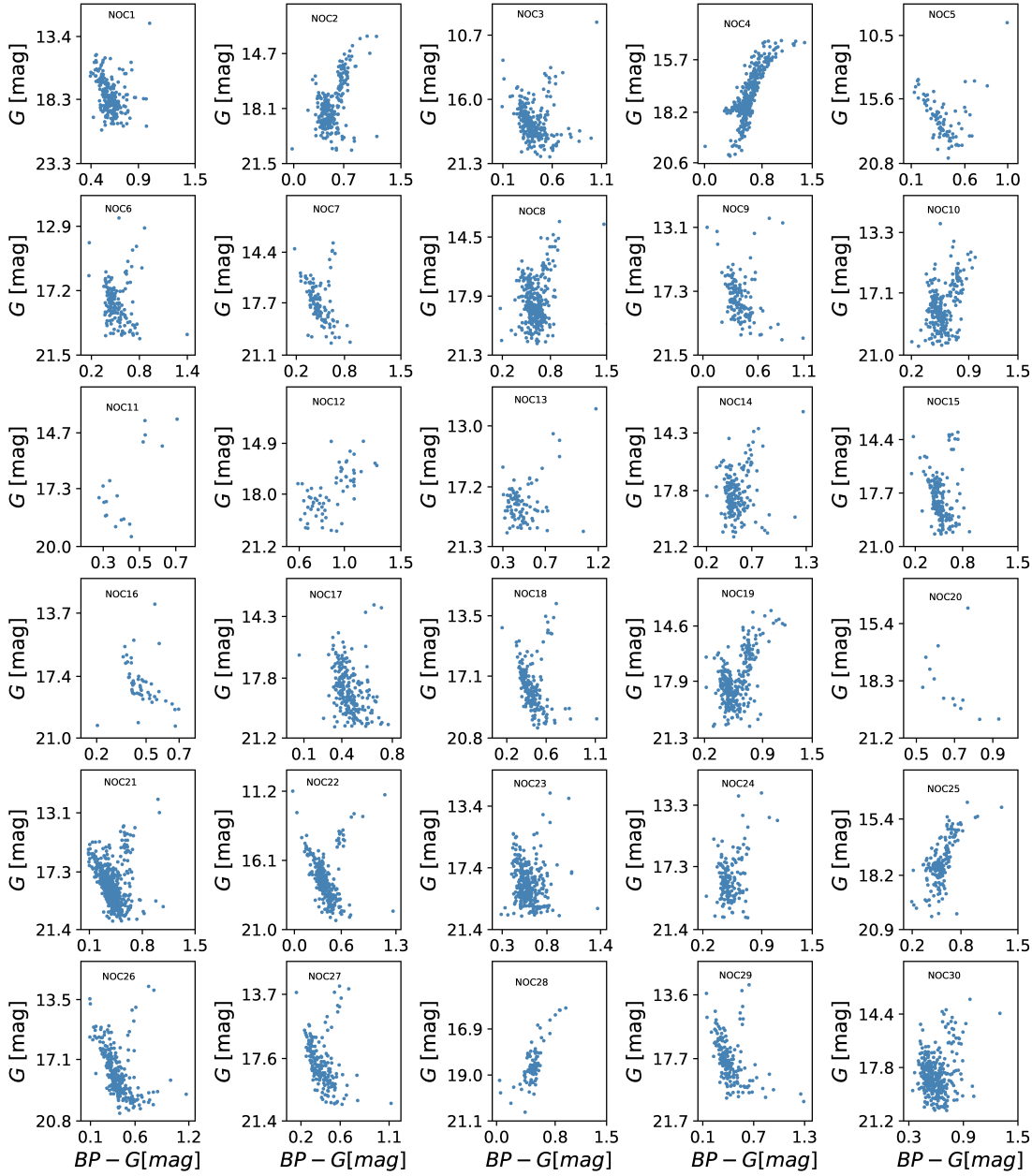


Fig. 12: CMDs of 30 newly found OCs with good CMDs. “BP” means “ G_{BP} ” magnitude.

their distributions are studied. Our results show a larger fraction of distant clusters comparing to previous work. The results can be used in many future studies, in particular the CMD studies. We can conclude that BSEC is a useful method of cluster identification, which helps for getting more precise CMDs, especially for clusters with small differential reddening. Although HDBSCAN and GMM blind search algorithms are used in this work, they can be changed to other ones. In fact, the results are somewhat sensitive to some adjustable parameters, which contributes to some clusters that are not recovered by this work. The method of EC can also be developed in the future.

Acknowledgements We appreciate the constructive comments of the referee, and thank Mr. Tao Xia and

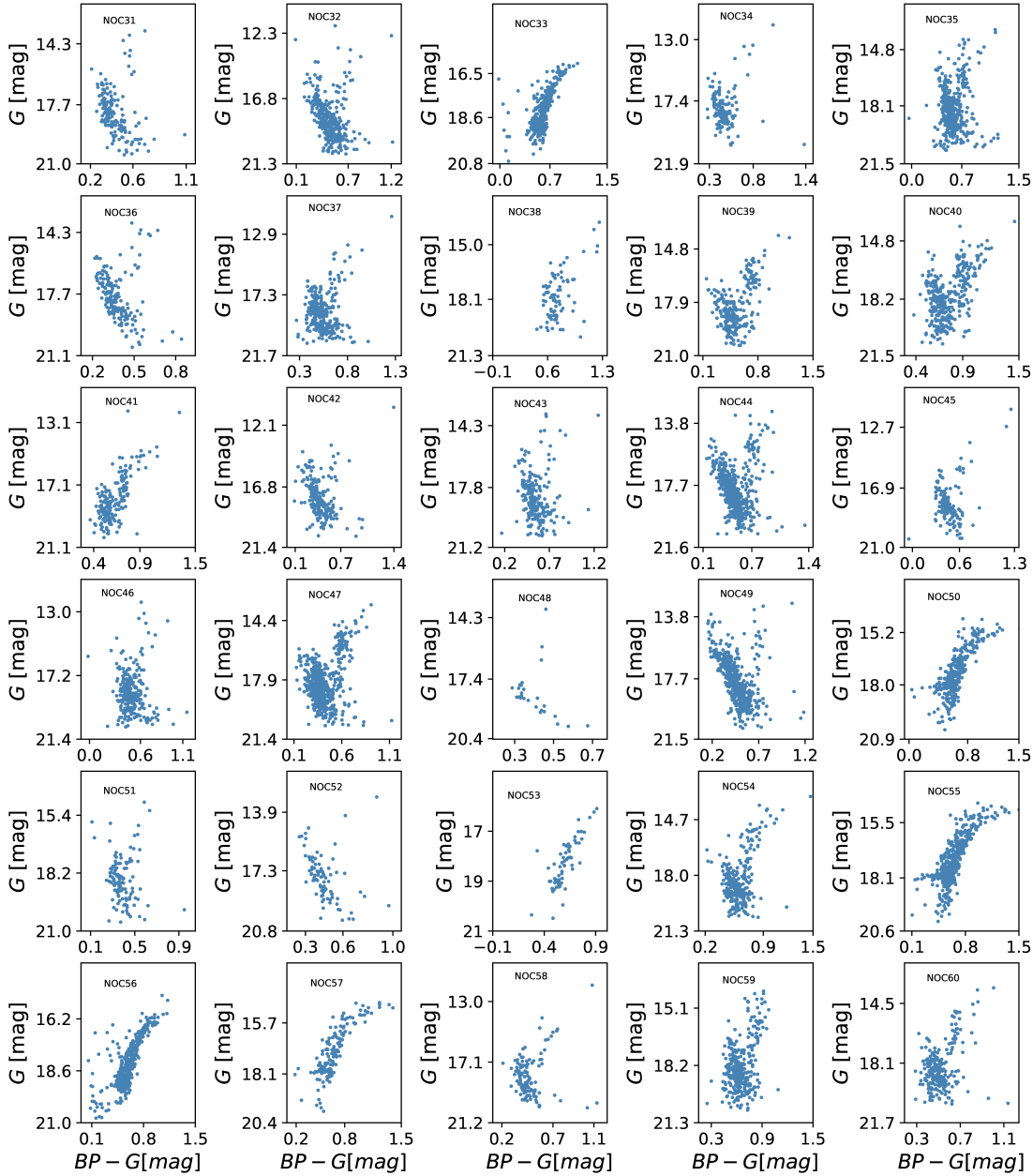


Fig. 13: Similar to Fig. 12, but for 30 other newly found OCs.

Jingxiu (202005AF150025) China Manned Space Project (NO.CMS-CSST-2021-A08), and GH project (ghfund202302019167).

This work has made use of data from the European Space Agency (ESA) mission *Gaia* (<https://www.cosmos.esa.int/gaia>), processed by the *Gaia* Data Processing and Analysis Consortium (DPAC, <https://www.cosmos.esa.int/web/gaia/dpac/consortium>). Funding for the DPAC has been provided by national institutions, in particular the institutions participating in the *Gaia* Multilateral Agreement.

DATA AVAILABILITY

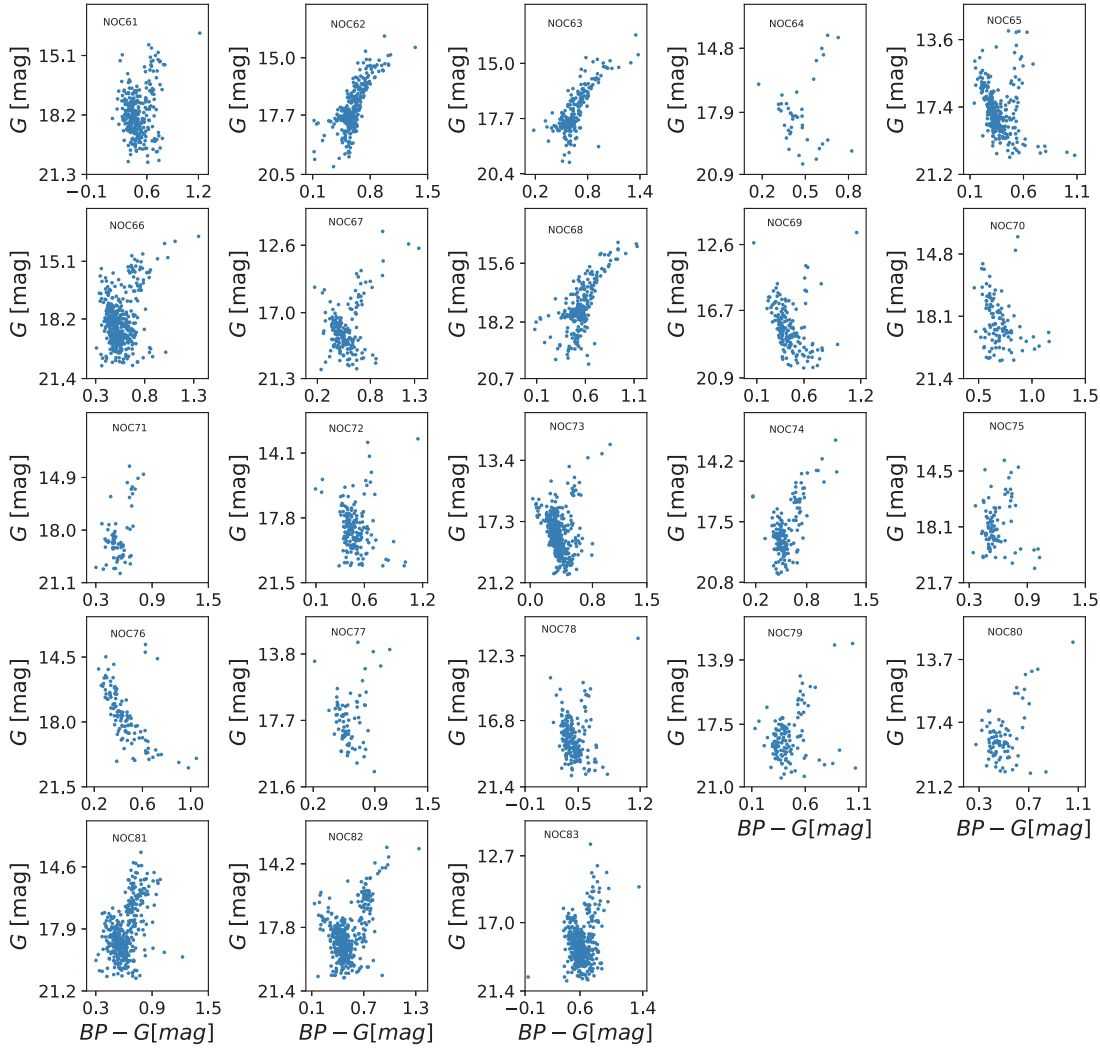


Fig. 14: Similar to Fig. 12, but for 23 other newly found OCs.

References

- Bica, E., Dutra, C. M., & Barbuy, B. 2003, *A&A*, 397, 177 9
- Bica, E., Santiago, B. X., Dutra, C. M., et al. 2001, *A&A*, 366, 827 9
- Camargo, D., Bica, E., & Bonatto, C. 2016a, *MNRAS*, 455, 3126 9
- Camargo, D., Bica, E., & Bonatto, C. 2016b, *A&A*, 593, A95 9
- Camargo, D., Bica, E., Bonatto, C., & Salerno, G. 2015, *MNRAS*, 448, 1930 9
- Campello, R. J. G. B., Moulavi, D., & Sander, J. 2013, in *Pacific-Asia Conference on Knowledge Discovery and Data Mining 2*
- Cantat-Gaudin, T., & Anders, F. 2020, *A&A*, 633, A99 9
- Cantat-Gaudin, T., Krone-Martins, A., Sedaghat, N., et al. 2019, *A&A*, 624, A126 2
- Cantat-Gaudin, T., Anders, F., Castro-Ginard, A., et al. 2020, *A&A*, 640, A1 9
- Castro-Ginard, A., Jordi, C., Luri, X., Cantat-Gaudin, T., & Balaguer-Nuñez, L. 2019, *A&A*, 627, A35 2, 9, 11

- Castro-Ginard, A., Jordi, C., Luri, X., et al. 2020, *A&A*, 635, A45 2, 9, 11
- Castro-Ginard, A., Jordi, C., Luri, X., et al. 2022, *A&A*, 661, A118 2, 9, 11
- Chen, L., Hou, J. L., & Wang, J. J. 2003, *AJ*, 125, 1397 9
- Chi, H., Wei, S., Wang, F., & Li, Z. 2023, *ApJS*, 265, 20 9
- Cummings, J. D., & Kalirai, J. S. 2018, *AJ*, 156, 165 7
- Damljanovic, G. 2021, in *XIX Serbian Astronomical Conference*, Vol. 100, 75 5
- Dempster, A. P., Laird, N. M., & Rubin, D. B. 1977, *Proceedings of the Royal Statistical Society*, 39, 1 2
- Dias, W. S., Alessi, B. S., Moitinho, A., & Lépine, J. R. D. 2002, *A&A*, 389, 871 9
- Dias, W. S., Monteiro, H., Moitinho, A., et al. 2021, *MNRAS*, 504, 356 9
- Ester, M., Kriegel, H. P., Sander, J., & Xu, X. 1996, *AAAI Press* 2
- Ferreira, F. A., Corradi, W. J. B., Maia, F. F. S., Angelo, M. S., & Santos, J. F. C., J. 2021, *MNRAS*, 502, L90 9
- Ferreira, F. A., Santos, J. F. C., Corradi, W. J. B., Maia, F. F. S., & Angelo, M. S. 2019, *MNRAS*, 483, 5508 9
- Forveille, T., & Kotak, R. 2021, *A&A*, 649, E1 5
- Frinchaboy, P. M., Majewski, S. R., Crane, J. D., et al. 2004, *ApJ*, 602, L21 9
- Gaia Collaboration, Prusti, T., de Bruijne, J. H. J., et al. 2016, *A&A*, 595, A1 2, 5
- Gaia Collaboration, Brown, A. G. A., Vallenari, A., et al. 2018, *A&A*, 616, A1 2, 5
- Gaia Collaboration, Brown, A. G. A., Vallenari, A., et al. 2021, *A&A*, 649, A1 2, 5
- Gaia Collaboration, Vallenari, A., Brown, A. G. A., et al. 2023, *A&A*, 674, A1 2, 5
- Glushkova, E. V., Kuposov, S. E., Zolotukhin, I. Y., et al. 2010, *Astronomy Letters*, 36, 75 9
- Hao, C. J., Xu, Y., Wu, Z. Y., et al. 2022, *A&A*, 660, A4 9
- Hao, C. J., Xu, Y., Hou, L. G., et al. 2021, *A&A*, 652, A102 2, 9
- He, Z.-H., Xu, Y., Hao, C.-J., Wu, Z.-Y., & Li, J.-J. 2021, *Research in Astronomy and Astrophysics*, 21, 093 2, 9
- He, Z., Wang, K., Luo, Y., et al. 2022a, *ApJS*, 262, 7 2, 9
- He, Z., Li, C., Zhong, J., et al. 2022b, *ApJS*, 260, 8 2, 9
- Hunt, E. L., & Reffert, S. 2021, *A&A*, 646, A104 2, 9
- Hunt, E. L., & Reffert, S. 2023, *A&A*, 673, A114 2, 6
- Kharchenko, N. V., Piskunov, A. E., Schilbach, E., Röser, S., & Scholz, R. D. 2013, *A&A*, 558, A53 2, 9
- Kos, J., de Silva, G., Buder, S., et al. 2018, *MNRAS*, 480, 5242 9
- Kounkel, M., & Covey, K. 2019, *AJ*, 158, 122 9
- Krone-Martins, A., & Moitinho, A. 2014, *A&A*, 561, A57 2
- Li, Z., Deng, Y., & Chen, J. 2021, *ApJS*, 253, 38 13
- Li, Z.-M., Mao, C.-Y., Luo, Q.-P., et al. 2017, *Research in Astronomy and Astrophysics*, 17, 071 13
- Li, Z., & Mao, C. 2023, *ApJS*, 265, 3 9
- Li, Z., Deng, Y., Chi, H., et al. 2022, *ApJS*, 259, 19 2, 9
- Liu, L., & Pang, X. 2019, *ApJS*, 245, 32 2
- Marigo, P., Girardi, L., Bressan, A., et al. 2017, *ApJ*, 835, 77 3, 6

- Mermilliod, J.-C. 1995, in *Information & On-Line Data in Astronomy*, ed. D. Egret & M. A. Albrecht, Vol. 203, 127 2
- Minniti, D. 2023, arXiv e-prints, arXiv:2306.12894 2
- Pera, M. S., Perren, G. I., Moitinho, A., Navone, H. D., & Vazquez, R. A. 2021, *A&A*, 650, A109 2
- Porras, A., Christopher, M., Allen, L., et al. 2003, *AJ*, 126, 1916 9
- Qin, S., Zhong, J., Tang, T., & Chen, L. 2023, *ApJS*, 265, 12 2, 9
- Reylé, C., & Robin, A. C. 2002, *A&A*, 384, 403 9
- Ryu, J., & Lee, M. G. 2018, *ApJ*, 856, 152 9
- Schmeja, S., Kharchenko, N. V., Piskunov, A. E., et al. 2014, *A&A*, 568, A51 9
- Scholz, R. D., Kharchenko, N. V., Piskunov, A. E., Röser, S., & Schilbach, E. 2015, *A&A*, 581, A39 9
- Sim, G., Lee, S. H., Ann, H. B., & Kim, S. 2019, *Journal of Korean Astronomical Society*, 52, 145 2
- Yang, X., Mo, H. J., van den Bosch, F. C., et al. 2005, *MNRAS*, 362, 711 2

Table 2: Number of cluster candidates that are crossmatched to different catalogs of known star clusters and candidates. They are shown in green in Fig. 5. Note that a few clusters or candidates in the catalogs of both this and previous works are closer than 0.5 deg, but they do not change the result obviously.

Serial Number	Catalog	Number
1	Bica et al. (2001)	1
2	Reyl & Robin (2002)	1
3	Dias et al. (2002)	1259
4	Bica et al. (2003)	31
5	Chen et al. (2003)	1
6	Porras et al. (2003)	5
7	Frinchaboy et al. (2004)	2
8	Kharchenko et al. (2013)	1685
9	Kharchenko et al. (2005)	617
10	Schmeja et al. (2014)	4
11	Scholz et al. (2015)	10
12	Camargo et al. (2016a)	232
13	Castro-Ginard et al. (2018)	19
14	Cantat-Gaudin et al. (2018)	794
15	Ryu & Lee (2018)	892
16	Cantat-Gaudin et al. (2019)	15
17	Castro-Ginard et al. (2019)	13
18	Kounkel & Covey (2019)	842
19	Liu & Pang (2019) (New OCs)	50
20	Ferreira et al. (2019)	3
21	Cantat-Gaudin & Anders (2020)	936
22	Castro-Ginard et al. (2020)	414
23	Cantat-Gaudin et al. (2020)	1324
24	Ferreira et al. (2020)	28
25	Hao et al. (2020)	3
26	Hunt & Reffert (2021)	28
27	Hao et al. (2021)	2143
28	Ferreira et al. (2021)	48
29	Dias et al. (2021)	1167
30	Hitchcock et al. (2021)	331
31	He et al. (2021)	45
32	Hao et al. (2022)	370
33	Castro-Ginard et al. (2022)	324
34	Li et al. (2022)	2577
35	He et al. (2022a)	255
36	Li & Mao (2023)	191
37	Chi et al. (2023a)	18
38	Chi et al. (2023b)	931
39	Milky Way globular clusters	298

Table 3: Similar to Table 1, but for 704 cluster candidates with good CMDs.

Serial Number	Catalog	Number
1	Dias et al. (2002)	185
2	Bica et al. (2003)	5
3	Kharchenko et al. (2005)	8
4	Kharchenko et al. (2013)	258
5	Scholz et al. (2015)	1
6	Camargo et al. (2016a)	27
7	Castro-Ginard et al. (2018)	5
8	Cantat-Gaudin et al. (2018)	144
9	Ryu & Lee (2018)	42
10	Castro-Ginard et al. (2019)	4
11	Kounkel & Covey (2019)	158
12	Liu & Pang (2019) (New OCs)	6
13	Cantat-Gaudin & Anders (2020)	177
14	Castro-Ginard et al. (2020)	61
15	Cantat-Gaudin et al. (2020)	236
16	Ferreira et al. (2020)	3
17	Hao et al. (2020)	1
18	Hunt & Reffert (2021)	3
19	Hao et al. (2021)	328
20	Dias et al. (2021)	218
21	He et al. (2021)	10
22	Hao et al. (2022)	35
23	Castro-Ginard et al. (2022)	43
24	Li et al. (2022)	355
25	He et al. (2022a)	35
26	Chi et al. (2023a)	5
27	Li & Mao (2023)	31
28	Chi et al. (2023b)	195
29	Milky Way globular clusters	43

Table 4: Example of known clusters that are not recovered by this work. In total, 2105 clusters are not recovered (see grey points in Fig. 5 for their distribution).

Name	l [deg]	b [deg]	Catalog
Berkeley 31	206.24	5.134	Cantat-Gaudin & Anders (2020)
Berkeley 59	121.3159	4.6454	Hitchcock et al. (2021)
Camargo 506	53.8	0.98	Camargo et al. (2016a)
CWNU5	176.325	-10.221	He et al. (2022a)
FSR 0555	128.809	8.64	Kharchenko et al. (2013)
LISC0115	93.5846	11.8759	Li et al. (2022)
LISC3630	300.835	-44.5	Li & Mao (2023)
Majaess 79	205.33	-2.696	Hao et al. (2021)
MBM 12	158.7839	-33.9554	Porras et al.(2003)
MWSC 5062	250.618	37.05	Schmeja et al. (2014)
NGC 7801	114.717	-11.331	Kharchenko et al. (2013)
Nor OB5	332.98	1.86	Kharchenko et al. (2005)
OC-0038	21.5732	-1.7624	Hao et al. (2022)
OC-13	38.7673	12.5237	Hao et al. (2020)
PHOC 7	47.2129	4.1091	Hunt & Reffert (2021)
RCW 40	220.79	-1.71	Reylé & Robin (2002)
Ryu001	336.7381	-4.9119	Ryu & Lee (2018)
SAI 2	120.5586	13.5431	Glushkova (2010)
Stock 21	120.118	-4.812	Hao et al. (2021)
UBC1133	89.67	2.7	Castro-Ginard et al. (2022)
UBC304	318.8354	-8.3884	Castro-Ginard et al. (2020)
UBC4	161.4289	-12.7555	Castro-Ginard et al. (2018), Kharchenko et al.(2013)
UBC85	126.0369	-4.8704	Castro-Ginard et al.(2019)
UFMG64	6.0804	2.9958	Ferreira et al. (2021)

Table 5: Astrometric parameters and their 1σ dispersions of 53 newly found OCs that the CMDs can be fitted well by isochrones. NOC ID is the serial number of the new OCs, while N_* is the number of member stars.

NOC ID	ra [deg]	dec [deg]	ϖ [mas]	$\mu_\alpha \cos\delta$ [mas/yr]	μ_δ [mas/yr]	N_*
1	293.543±0.159	12.677±0.148	0.310±0.045	-2.832±0.262	-5.344±0.274	220
2	178.725±0.175	-67.949±0.178	0.081±0.040	-6.249±0.284	1.240±0.236	258
3	120.966±0.170	-20.028±0.178	0.196±0.113	-1.386±0.254	1.098±0.121	283
4	286.079±0.162	-30.500±0.166	0.042±0.026	-2.690±0.164	-1.460±0.160	446
5	99.286±0.146	22.987±0.148	0.264±0.116	-0.241±0.079	-1.243±0.273	83
6	330.097±0.170	46.574±0.154	0.224±0.129	-2.532±0.100	-2.949±0.292	153
7	92.271±0.153	40.870±0.173	0.256±0.115	0.385±0.098	-1.604±0.270	116
8	295.919±0.167	9.461±0.162	0.211±0.113	-3.024±0.109	-5.063±0.276	310
9	113.852±0.170	-0.275±0.174	0.298±0.120	-1.182±0.104	-0.199±0.282	136
10	295.567±0.163	13.756±0.137	0.179±0.089	-3.051±0.099	-4.980±0.299	245
11	57.972±0.149	27.059±0.123	0.103±0.038	0.057±0.283	-0.493±0.112	18
12	256.578±0.096	-49.406±0.121	0.122±0.067	-2.453±0.272	-4.299±0.280	68
13	130.354±0.175	-60.519±0.172	0.206±0.106	-3.056±0.108	4.252±0.291	90
14	297.941±0.190	12.920±0.124	0.205±0.099	-3.187±0.289	-5.016±0.118	187
15	140.935±0.155	-41.179±0.154	0.227±0.130	-4.016±0.097	2.980±0.291	170
16	88.220±0.167	53.178±0.150	0.214±0.097	0.459±0.187	-1.644±0.249	50
17	103.114±0.161	-21.458±0.165	0.313±0.052	-0.045±0.252	1.369±0.293	230
18	92.743±0.181	37.855±0.180	0.256±0.141	0.822±0.106	-1.562±0.282	177
19	171.677±0.128	-57.142±0.113	0.105±0.050	-5.271±0.287	1.364±0.278	292
20	11.047±0.165	78.595±0.167	0.174±0.063	-1.088±0.228	0.909±0.199	13
21	107.895±0.171	-27.265±0.169	0.158±0.099	-0.632±0.239	1.977±0.086	545
22	113.097±0.153	-8.869±0.147	0.198±0.107	-0.871±0.095	0.808±0.275	294
23	292.381±0.160	7.860±0.175	0.354±0.051	-3.128±0.270	-5.741±0.279	314
24	184.355±0.176	-54.502±0.177	0.209±0.122	-5.818±0.086	0.337±0.286	158
25	290.258±0.157	-33.003±0.161	0.050±0.031	-2.632±0.188	-1.489±0.157	203
26	114.366±0.170	-9.054±0.150	0.239±0.129	-1.187±0.112	0.647±0.252	252
27	129.249±0.175	-29.224±0.140	0.242±0.114	-2.648±0.109	2.856±0.284	181
28	80.373±0.109	-61.864±0.166	0.048±0.031	1.658±0.172	0.341±0.143	88
29	114.009±0.172	-3.940±0.168	0.214±0.121	-1.370±0.108	0.478±0.280	175
30	310.911±0.165	33.306±0.166	0.228±0.135	-3.266±0.103	-4.561±0.273	345
31	130.919±0.181	-29.677±0.169	0.149±0.082	-2.546±0.148	2.513±0.287	157
32	115.803±0.160	-16.760±0.151	0.223±0.126	-1.026±0.100	1.262±0.284	316
33	74.994±0.164	-73.588±0.170	0.035±0.022	2.066±0.164	0.023±0.180	386
34	331.750±0.194	47.690±0.174	0.189±0.075	-2.222±0.185	-2.578±0.132	131
35	300.381±0.167	17.852±0.167	0.223±0.122	-2.813±0.106	-4.840±0.289	400
36	125.075±0.173	-23.856±0.166	0.115±0.055	-2.122±0.184	2.116±0.296	182
37	168.643±0.179	-53.381±0.174	0.222±0.128	-5.727±0.281	1.392±0.123	266
38	280.126±0.145	-18.827±0.156	0.261±0.121	-1.527±0.113	-4.148±0.302	81
39	123.397±0.171	-49.160±0.174	0.069±0.036	-1.727±0.157	2.782±0.264	243
40	290.702±0.146	24.655±0.168	0.162±0.091	-2.533±0.246	-5.288±0.112	345
41	279.433±0.163	8.508±0.131	0.076±0.041	-2.157±0.281	-4.766±0.294	182
42	99.921±0.169	22.927±0.175	0.217±0.118	0.118±0.255	-0.996±0.122	210
43	343.851±0.172	53.177±0.169	0.222±0.120	-1.780±0.101	-1.461±0.283	210
44	124.006±0.169	-29.385±0.164	0.117±0.053	-1.853±0.261	2.082±0.270	568
45	97.509±0.176	28.688±0.169	0.093±0.049	0.076±0.265	-1.363±0.263	140
46	300.823±0.171	13.652±0.173	0.225±0.122	-2.688±0.110	-4.665±0.283	254
47	118.493±0.176	-44.822±0.176	0.084±0.041	-1.348±0.245	2.870±0.276	576
48	6.326±0.190	-72.710±0.068	0.180±0.095	5.431±0.147	-2.579±0.148	26
49	112.340±0.175	-10.282±0.177	0.231±0.125	-1.148±0.248	0.838±0.109	470

Table 6: Similar to Table 5, but for other 30 new OCs.

NOC ID	ra [deg]	dec [deg]	ϖ [mas]	$\mu_\alpha \cos\delta$ [mas/yr]	μ_δ [mas/yr]	N_*
54	185.175±0.162	-55.833±0.161	0.098±0.052	-6.135±0.273	0.369±0.278	264
55	284.427±0.170	-31.108±0.170	0.040±0.024	-2.650±0.137	-1.391±0.132	598
56	72.695±0.173	-73.410±0.175	0.038±0.023	2.036±0.181	-0.094±0.172	428
57	281.877±0.180	-31.218±0.176	0.026±0.014	-2.623±0.131	-1.388±0.107	161
58	303.148±0.181	52.038±0.145	0.116±0.060	-2.643±0.197	-3.736±0.251	122
59	300.908±0.154	21.728±0.115	0.113±0.053	-3.060±0.280	-5.512±0.279	330
60	334.451±0.178	48.697±0.175	0.087±0.046	-2.047±0.281	-2.140±0.282	245
61	137.442±0.168	-55.768±0.100	0.176±0.109	-3.198±0.265	3.721±0.127	283
62	284.360±0.163	-32.088±0.160	0.049±0.029	-2.675±0.185	-1.397±0.150	357
63	283.578±0.186	-28.571±0.176	0.036±0.022	-2.702±0.179	-1.441±0.152	212
64	11.345±0.159	46.719±0.163	0.172±0.068	-1.287±0.284	-1.115±0.253	40
65	108.049±0.174	6.831±0.177	0.197±0.112	-0.216±0.253	-0.403±0.106	265
66	311.936±0.164	35.054±0.158	0.192±0.113	-2.564±0.260	-3.991±0.111	414
67	338.903±0.153	52.483±0.165	0.099±0.053	-1.985±0.279	-1.605±0.153	182
68	286.581±0.152	-32.827±0.152	0.057±0.035	-2.665±0.169	-1.380±0.161	243
69	117.597±0.174	-11.972±0.166	0.217±0.133	-1.361±0.266	1.164±0.124	162
70	275.711±0.174	4.274±0.174	0.400±0.067	-2.306±0.274	-5.223±0.280	113
71	274.396±0.131	5.510±0.104	0.173±0.109	-1.914±0.245	-5.811±0.108	68
72	134.480±0.172	-32.839±0.169	0.230±0.123	-2.156±0.270	2.016±0.127	165
73	106.496±0.175	-28.987±0.171	0.176±0.112	-0.795±0.103	1.938±0.259	399
74	297.140±0.167	12.224±0.168	0.096±0.040	-2.594±0.264	-5.218±0.240	153
75	255.013±0.119	-53.853±0.188	0.249±0.151	-3.455±0.101	-5.025±0.287	93
76	90.543±0.163	47.532±0.161	0.258±0.087	0.475±0.115	-1.606±0.278	112
77	209.252±0.152	-67.055±0.118	0.228±0.085	-6.121±0.291	-2.787±0.135	78
78	151.382±0.150	-47.290±0.166	0.220±0.124	-5.018±0.109	3.074±0.280	182
79	340.376±0.131	48.294±0.165	0.094±0.047	-1.747±0.259	-1.797±0.260	124
80	125.771±0.150	-58.330±0.169	0.120±0.053	-2.535±0.289	3.883±0.281	85
81	294.135±0.154	7.751±0.167	0.097±0.052	-2.632±0.291	-5.201±0.274	373
82	112.327±0.163	-36.279±0.159	0.099±0.044	-0.910±0.250	2.240±0.273	417
83	303.025±0.162	23.490±0.172	0.200±0.118	-2.598±0.099	-4.998±0.288	391